Research article JHEP|Reports

AKR1B1 drives hyperglycemia-induced metabolic reprogramming in MASLD-associated hepatocellular carcinoma

Authors

NP Syamprasad, Siddhi Jain, Bishal Rajdev, Samir Ranjan Panda, Gangasani Jagadeesh Kumar, Khaja Moinuddin Shaik, P.A. Shantanu, Veerabhadra Swamy Challa, Sachin B. Jorvekar, Roshan M. Borkar, Jayathirtha Rao Vaidya, Dinesh Mani Tripathi, V.G.M. Naidu

Correspondence

vgmnaidu@gmail.com, vgmnaidu@niperguwahati.ac.in (V.G.M. Naidu), dineshmanitripathi@gmail.com (D.M. Tripathi).

Graphical abstract

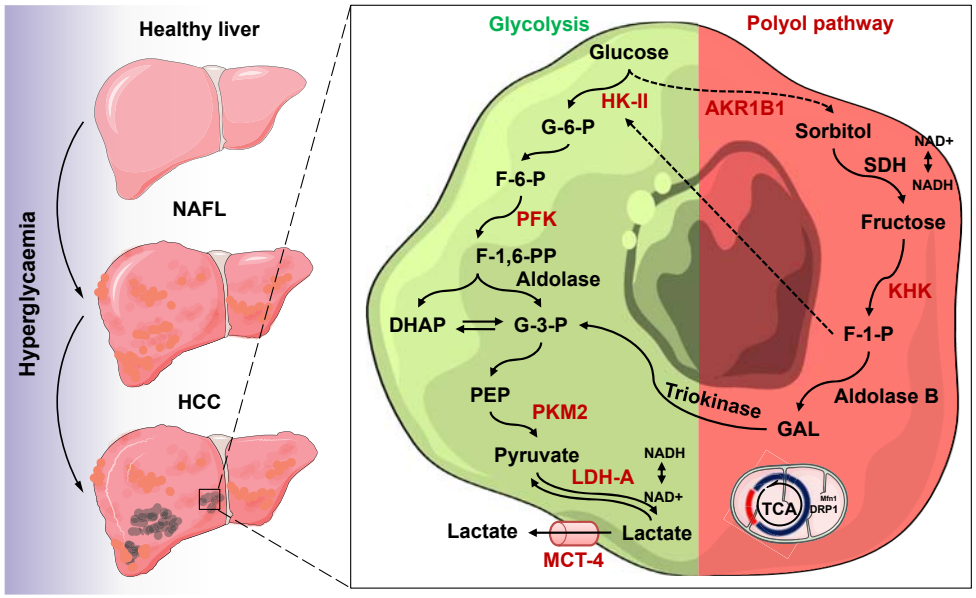

Highlights

- Pathological AKR1B1 modulates hepatic metabolism to promote MASLD-associated hepato-carcinogenesis.
- AKR1B1 is associated with the promotion of the Warburg effect in HCC.
- AKR1B1 levels in plasma could act as a prognostic marker and diagnostic test for MASLD and associated HCC.
- Aldose reductase inhibition modulates the glycolytic pathway to prevent pre-cancerous hepatocyte formation.
- NARI-29 can be developed as a promising ARI for the treatment of MASLD and associated HCC.

Impact and implications

This research work highlights AKR1B1 as a druggable target in metabolic dysfunction-associated steatotic liver disease (MASLD) and hepatocellular carcinoma (HCC), which could provide the basis for the development of new chemotherapeutic agents. Moreover, our results indicate the potential of plasma AKR1B1 levels as a prognostic marker and diagnostic test for MASLD and associated HCC. Additionally, a major observation in this study was that AKR1B1 is associated with the promotion of the Warburg effect in HCC.

https://doi.org/10.1016/j.jhepr.2023.100974

Research article

JHEP|Reports

AKR1B1 drives hyperglycemia-induced metabolic reprogramming in MASLD-associated hepatocellular carcinoma

NP Syamprasad,[1] Siddhi Jain,[1] Bishal Rajdev,[1] Samir Ranjan Panda,[1] Gangasani Jagadeesh Kumar,[1] Khaja Moinuddin Shaik,[1] P.A. Shantanu,[1] Veerabhadra Swamy Challa,[1] Sachin B. Jorvekar,[2] Roshan M. Borkar,[2] Jayathirtha Rao Vaidya,[4] Dinesh Mani Tripathi,[3,*] V.G.M. Naidu[1,*]

[1]*Department of Pharmacology & Toxicology, National Institute of Pharmaceutical Education and Research Guwahati, Sila village, Changsari, Assam, 781101, India;* [2]*Department of Pharmaceutical Analysis, National Institute of Pharmaceutical Education and Research Guwahati, Sila village, Changsari, Assam, 781101, India;* [3]*Liver Physiology & Vascular Biology Lab, Department of Molecular and Cellular Medicine, Institute of Liver and Biliary Sciences, ILBS, D-1, Vasant Kunj, New Delhi, Delhi 110070, India;* [4]*Fluoro Agro Chemicals Department and AcSIR-Ghaziabad, CSIR-Indian Institute of Chemical Technology, Uppal Road Tarnaka, Hyderabad, Telangana, 500007, India*

JHEP Reports **2024.** https://doi.org/10.1016/j.jhepr.2023.100974

Background & Aims: The mechanism behind the progressive pathological alteration in metabolic dysfunction-associated steatotic liver disease/steatohepatitis (MASLD/MASH)-associated hepatocellular carcinoma (HCC) is poorly understood. In the present study, we investigated the role of the polyol pathway enzyme AKR1B1 in metabolic switching associated with MASLD/MASH and in the progression of HCC.

Methods: AKR1B1 expression was estimated in the tissue and plasma of patients with MASLD/MASH, HCC, and HCC with diabetes mellitus. The role of AKR1B1 in metabolic switching *in vitro was* assessed through media conditioning, lentiviral transfection, and pharmacological probes. A proteomic and metabolomic approach was applied for the in-depth investigation of metabolic pathways. Preclinically, mice were subjected to a high-fructose diet and diethylnitrosamine to investigate the role of AKR1B1 in the hyperglycemia-mediated metabolic switching characteristic of MASLD-HCC.

Results: A significant increase in the expression of AKR1B1 was observed in tissue and plasma samples from patients with MASLD/MASH, HCC, and HCC with diabetes mellitus compared to normal samples. Mechanistically, *in vitro* assays revealed that AKR1B1 modulates the Warburg effect, mitochondrial dynamics, the tricarboxylic acid cycle, and lipogenesis to promote hyperglycemia-mediated MASLD and cancer progression. A pathological increase in the expression of AKR1B1 was observed in experimental MASLD-HCC, and expression was positively correlated with high blood glucose levels. High-fructose diet + diethylnitrosamine-treated animals also exhibited statistically significant elevation of metabolic markers and carcinogenesis markers. AKR1B1 inhibition with epalrestat or NARI-29 inhibited cellular metabolism in *in vitro* and *in vivo* models.

Conclusions: Pathological AKR1B1 modulates hepatic metabolism to promote MASLD-associated hepatocarcinogenesis. Aldose reductase inhibition modulates the glycolytic pathway to prevent precancerous hepatocyte formation.

Impact and implications: This research work highlights AKR1B1 as a druggable target in metabolic dysfunction-associated steatotic liver disease (MASLD) and hepatocellular carcinoma (HCC), which could provide the basis for the development of new chemotherapeutic agents. Moreover, our results indicate the potential of plasma AKR1B1 levels as a prognostic marker and diagnostic test for MASLD and associated HCC. Additionally, a major observation in this study was that AKR1B1 is associated with the promotion of the Warburg effect in HCC.

© 2023 The Authors. Published by Elsevier B.V. on behalf of European Association for the Study of the Liver (EASL). This is an open access article under the CC BY-NC-ND license (http://creativecommons.org/licenses/by-nc-nd/4.0/).

Introduction

The quality of human life is dependent on lifestyle and food habits. Modernized diets high in carbohydrate and fat but low in protein and fiber result in chronic metabolic disorders.[1,2] Cumulated evidence suggests a strong relationship between unhealthy food habits and the development and progression of numerous cancers.[3] One typical example is the development of hepatocellular carcinoma (HCC) from metabolic dysfunction-associated steatotic liver disease (MASLD) or metabolic dysfunction-associated steatohepatitis (MASH) (formally NAFLD or NASH[4]). Studies suggest that high glucose (HG) and fructose intake are associated with an increased risk of HCC, and hyperglycemia is considered a prognostic factor in HCC.[5,6] Altered metabolic pathways associated with high dietary glycemic load drive HCC into a more aggressive phenotype resulting in chemoresistance and metastasis.[7]

One well-defined metabolic change termed the Warburg effect is a process in which cancer cells undergo glycolysis even in

Keywords: MASLD/MASH; HCC; Metabolism; Warburg effect; NARI-29; epalrestat; high fructose diet; diethyl nitrosamine.

Received 2 February 2023; received in revised form 21 October 2023; accepted 25 October 2023; available online 28 November 2023

* Corresponding authors. Addresses: National Institute of Pharmaceutical Education and Research, Changsari, Guwahati, Assam, 781101, India. (V.G.M. Naidu) or Department of Molecular and Cellular Medicine, Institute of Liver and Biliary Sciences, ILBS, D-1, Vasant Kunj, New Delhi, Delhi 110070, India; (D.M. Tripathi).

E-mail addresses: vgmnaidu@gmail.com, vgmnaidu@niperguwahati.ac.in (V.G.M. Naidu), dineshmanitripathi@gmail.com (D.M. Tripathi).

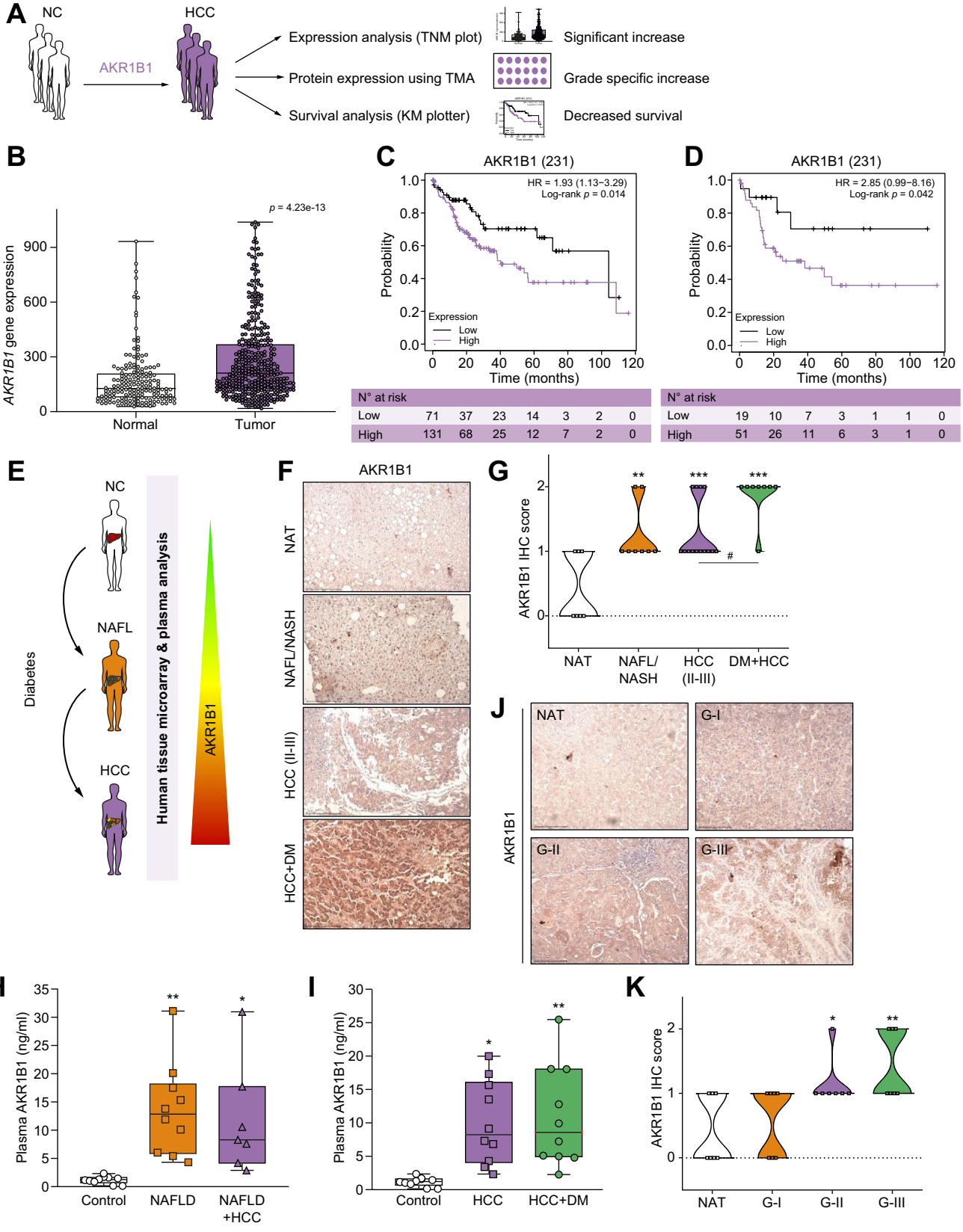

Fig. 1. AKR1B1 associates with MASLD/MASH, HCC, and DM+HCC progression. (A) Pictorial representation of study outline. (B) *AKR1B1* gene expression in normal and HCC tumor samples using TNM plot. Survival analysis of patients with non-alcohol-related HCC in (C) all stages and (D) stage 3. (E). Study design for clinical sample analysis. (F) Immunohistochemistry and (G) violin plots for AKR1B1 expression in MASH/MASLD, HCC, and DM+HCC (each dot represents individual data, and joints represent median values). Level of significance: $^{**}p$ <0.01, $^{***}p$ <0.0001, *and* $^{\#}$ p <0.05 (one-way ANOVA followed by Tukey test). Plasma

abundant oxygen (aerobic glycolysis).[8] Even though the Warburg effect produces less ATP than oxidative phosphorylation, the fermentation product lactate will favor cancer progression by creating a tumor microenvironment. Moreover, lactate secreted from glycolytic cancer cells is a reserved energy source for oxidative cancer cells.[9] Typically, cancer cells lacking adequate glucose supply gradually deplete their energy and undergo apoptosis, but lactate secreted by glycolytic cancer cells can serve as an energy source for other cells and be converted to pyruvate by reverse glycolysis.[10] This pyruvate enters oxidative phosphorylation to produce energy and promote survival of cancer cells without a nutrient supply. Interestingly, a similar metabolic phenotype is observed in hepatocytes from patients with MASLD and MASH.[1] Hence, identifying the underlying cause of metabolic switching will help to prevent and treat HCC. Recent studies suggest that increased fructose production in the liver induces hepatic fat accumulation and yields uric acid, which is highly associated with MASLD and MASH.[11] Clinical reports also indicate that the overexpression of aldose reductase genes was evident in patients with MASH.[12] There is growing epidemiological proof that MASLD and MASH have turned out to be the leading etiology for many cases of HCC.[13]

Levels of the polyol pathway master regulator AKR1B1 are low in normal tissues, but in hyperglycemic conditions AKR1B1 is overexpressed and drives 30-50% of glucose to the polyol pathway. Increased polyol flux leads to the conversion of glucose to sorbitol and fructose, which are responsible for diabetic complications such as nephropathy, neuropathy, and cataracts.[14] Moreover, there is strong evidence that aldose reductase promotes HCC progression by interacting with various signaling pathways[15] and the byproduct of polyol flux, fructose, can trigger fatty liver disease through metabolic modulation. Despite being a metabolic modulator in diabetic conditions, the pathological role of AKR1B1 in MASLD and HCC under hyperglycemia is unknown. Hence, in the present study, we have investigated the role of AKR1B1 in hyperglycemia-augmented MASLD-associated hepatocarcinogenesis and hepatic cancer progression with the aid of human tissue and plasma samples, genetic manipulation, and small molecule inhibitors. Preclinically, the aldose reductase inhibitor epalrestat (EPS) and the specific AKR1B1 inhibitor NARI-29[16–19] were employed to elucidate the effect of pharmacological inhibition of AKR1B1.

Materials and methods

Clinical specimens and bioinformatics

The plasma and slides of normal adjacent tissue, MASLD/MASH, HCC, and diabetes mellitus (DM)+HCC (DM+HCC) were obtained from the National Liver Disease Biobank, Institute of Liver & Biliary Sciences, New Delhi, India, with informed consent under the institutional review board (IEC/2023/98/MA05). Survival analysis (based on AKR1B1 expression) and an analysis of the differential expression of AKR1B1 between tumor/non-tumor tissue in patients with non-alcohol-related liver cancer was performed using RNA-Seq data from the Kaplan-Meier plotter, and TNM plot.[20] A detailed description is provided in the supplementary methods.

Cell culture experiments and transfection

All the cells were purchased from the ATCC (American Type Culture Collection) and maintained according to ATCC guidelines. HepG2 cells were cultured in a medium containing 4.5 g/L glucose for the hyperglycemic condition experiments. AKR1B1 was overexpressed in PLC/PRF-5 cells using the Human Tagged ORF Clone Lentiviral Particle (Origene-RC200504L4V) to study its effect on metabolic reprogramming in hepatic cancer. Detailed descriptions of *in vitro* experiments are given in the supplementary methods.

Animal experiments

Animal experiments were performed according to the CPCSEA (Committee for the purpose of control and supervision of experiments on animals) guidelines and were approved by the IAEC (institutional animal ethical committee) with protocol number NIPER/PC/2022/45. The design for the *in vivo* study is depicted in Fig. 7A. A detailed description of animal model development and treatments is provided in the supplementary methods.

Statistical analysis

Unless mentioned, the data are expressed as mean (SEM) of minimum triplicate experiments. All statistical analysis was performed using GraphPad Prism software 8.0 version. *P* values were determined using one-way ANOVA or two-way ANOVA followed by Tukey's multiple comparison tests depending on the dataset.

Results

AKR1B1 associated with progression of MASLD/MASH, HCC, and DM+HCC

The mRNA expression data from the TNM plot reveals a significant difference in the expression of *AKR1B1* in tumor samples of HCC compared to normal liver samples (Fig. 1B). Moreover, the Kaplan-Meier plotter indicated that overexpression of *AKR1B1* results in worse overall survival outcomes in patients with HCC (Fig. 1C; all grades and Fig. 1D; grade 3). Further, as shown in Fig. 1F,G, immune-positivity of AKR1B1 was significantly higher in tissue sections of MASLD/MASH (p <0.01), HCC (p <0.001), and DM+HCC (p <0.001) compared to normal adjacent tissues. This data indicates that AKR1B1 could be a major contributing factor in the progression of MASLD/MASH to HCC. Similarly, plasma levels of AKR1B1 were significantly elevated in patients with MASLD (p <0.01) and MASLD-associated HCC (p <0.05) compared to healthy individuals (Fig. 1H). Most importantly, as depicted in Fig. 1F,G, we could observe a significant elevation in AKR1B1 expression in DM+HCC compared to HCC alone (p <0.05), which correlated with the plasma levels of AKR1B1 (Fig. 1I). Furthermore, the immunohistochemistry scoring of AKR1B1 expression was significantly higher in grade 2 (p <0.05) and grade 3 (p <0.01)

expression of AKR1B1 in (H) MASLD and MASLD+HCC compared with normal control and (I) HCC and DM+HCC compared with normal control. Level of significance: $^{*}p$ <0.05, $^{**}p$ <0.01; (one-way ANOVA followed by Tukey test). (J, K) expression of AKR1B1 in different stages of HCC. Data is represented as mean±SEM (n ≥6). Each dot represents individual data and the line inside the box represents median values. Level of significance: $^{*}p$ <0.05, $^{**}p$ <0.01; (one-way ANOVA followed by Tukey test). DM, diabetes mellitus; HCC, hepatocellular carcinoma; NAFLD, non-alcoholic fatty liver disease; NASH, non-alcoholic steatohepatitis; NAT, normal adjacent tissue.

HCC compared to non-cancerous samples. Cumulatively, the data suggests the role of AKR1B1 as a disease-progressive marker in MASLD/MASH, MASLD-associated HCC, and DM-aggravated HCC progression. Plasma estimation of AKR1B1 could be a predictive method for the early identification of liver ailments such as MASLD and its progression to MASH and HCC.

AKR1B1 overexpression is associated with modulation of glycolytic markers in HCC under hyperglycemic conditions

We have used various cell culture systems and experiments to delineate the role of AKR1B1 in hyperglycemia-aggravated MASLD/MASH and HCC progression (Fig. 2A). As shown in Fig. 2B, AKR1B1 expression was highest in the HepG2 cell line among other hepatic cancer cell lines, where SNU-387 and HEPA 1-6 cell lines have a moderate expression of AKR1B1. Around a 20-fold change in expression was observed in the HepG2 cell line compared to hepatic fibroblast cell line BRL-3A. In contrast, poorly differentiated hepatic cancer cell line PLC/PRF-5 has minimal expression of AKR1B1 compared to other cancer cell lines. A significant increase in lactate secretion was observed in HepG2 (p <0.001), SNU 387 (p <0.01), and HEPA 1-6 (p <0.001) cells. However, no significant change in the secretion of lactate was observed in PLC/PRF-5 and BRL-3A cell lines (Fig. 2C), which express low levels of AKR1B1, showing that AKR1B1 might be responsible for the Warburg effect in hepatic cancer. Moreover, a considerable increase in the expression of AKR1B1 (p <0.001) was witnessed in the HepG2 cells cultured in HG media (Figs 2D, E, and S1A), which could be responsible for the overexpression of glycolytic enzymes cMYC (p <0.01), hexokinase-II (HK-II) (p <0.001), ketohexokinase (KHK) (p <0.001), lactate dehydrogenase A (LDHA) (p <0.05), and monocarboxylate transporter-4 (MCT-4) (p <0.01), modulating the Warburg effect (Fig. 2G, H).

Further, Oil Red O (ORO) staining revealed that the HepG2 cells were presented with high lipid droplets (p <0.001) under hyperglycemia, and treatment with BSA-PA (500 μM) has further enhanced the production of oil globules. However, oil deposition in low glucose (LG) media is lower (p <0.01) than in HG media (p <0.001), indicating that AKR1B1 could be a contributing factor for hyperglycemia-mediated fatty liver progression (Figs 2F and 5G). Moreover, we have observed significantly increased (p <0.01) wound closure in HepG2 cells cultured in HG media over LG media, demonstrating the role of AKR1B1 in the hyperproliferation and metastasis of HCC (Fig. S1B).

Lentiviral transfection of huAKR1B1 leads to metabolic reprogramming in PLC/PRF-5 cell line

To delineate the exact role of AKR1B1 in metabolic modulation and the Warburg effect, we have stably transfected AKR1B1 low-expressing PLC/PRF-5 cells with lentiviral particles. As shown in Fig. 2I, we obtained PLC/PRF-5 cells stably overexpressing AKR1B1 at a multiplicity of infection of 20. The flow cytometric measurement of mGFP in non-transfected and transfected cells showing a 30-fold difference in green fluorescence emission further confirms the transfection efficiency (Fig. S2). As presented in Fig. 2J-L, overexpression of AKR1B1 (p <0.001) leads to upregulation of cMYC (p <0.01), HK-II (p <0.01), KHK (p <0.001), and LDHA (p <0.001) like that observed in the hyperglycemic condition. The increase in lactate secretion (p <0.001) (Fig. 2M) confirmed the modulation of metabolic reprogramming and the Warburg effect in PLC/PRF-5-AKR1B1+ cells compared to wild-type PLC/PRF-5 cells under normal and HG conditions.

AKR1B1 inhibition by small molecules represses polyol flux and glucose transporter to prevent hepatic cancer cell proliferation

Previously, it has been reported that NARI-29 is a structural analog of EPS with more potent AKR1B1 inhibition.[19] Hence, in the present study, we have used EPS and NARI-29 as pharmacological probes to elucidate the role of AKR1B1 in metabolic reprogramming. Initially, we demonstrated that NARI-29 and EPS dose-dependently reduced the proliferation of hepatic cancer cell lines, and their cytotoxicity is directly correlated with AKR1B1 expression. As shown in Fig. 3A, NARI-29 exhibited cytotoxicity in HepG2, SNU-475, and SK-Hep1 cells, with IC50 values of 6.6, 7.1, and 15.1 μM, respectively. EPS showed EC_{50} values of 58.7, 78.7, and 77.1 μM in respective cell lines. Interestingly, NARI-29 and EPS failed to induce significant cytotoxicity on the PLC/PRF-5 cell line (Fig. 3A), primary mouse hepatocytes, peripheral blood mononuclear cells, and red blood cells (Fig. S3). However, NARI-29 and EPS prevented the AKR1B1 overexpression-mediated hyper-proliferation of PLC/PRF-5-AKR1B1+ cells, thus eliciting increased growth inhibition than in wild-type PLC/PF-5 cells (IC_{50} values of 55.69 and 223.89 μM, respectively) (Fig. 2N). Moreover, AKR1B1 inhibition with EPS (50 μM), and NARI-29 (10 μM) in HepG2 cells cultured in HG media resulted in cell cycle arrest at the G2/M phase (Fig. S4), reduced proliferation, and metastasis (Fig. S5). As shown in Fig. 3C, AKR1B1 inhibition also induced toxicity to HepG2 spheroids cultured in HG media. FDA/PI staining indicated significant cell death in EPS- or NARI-29-treated groups compared to untreated groups (p <0.001).

Further, we investigated the fate of metabolic enzymes in hyperglycemia after AKR1B1 inhibition in HepG2 and PLC/PRF-5-AKR1B1+ cells. Immuno-fluorescence (Fig. 3D) and immunoblotting (Fig. 3F) data advise that AKR1B1 inhibition with NARI-29 at 10 and 20 μM concentrations has significantly reduced the expression of KHK (p <0.001), which converts fructose to fructose-1-phosphate in the HepG2 cell line under hyperglycemic conditions. Even though 50 μM of EPS has considerably reduced the expression of KHK (p <0.05), the effect was less than the low dose of NARI-29. Similarly, in PLC/PRF-5-AKR1B1+ cells, 50 μM of NARI-29 significantly (p <0.01) reduced the expression of KHK compared to EPS at 200 μM (p <0.05) (Fig. 3B, E), indicating the potency of NARI-29 over EPS in the inhibition of polyol flux and the rerouting of fructose to the glycolytic pathway. Further, AKR1B1 inhibition inhibited the phosphorylation of Akt (NARI L; p <0.001, NARI H; p <0.001, and EPS; p <0.001) and inhibited cMYC (NARI L; p <0.05, NARI H; p <0.01, and EPS; p <0.05), which leads to downregulation of glucose transporter 1 (NARI L; p <0.05, NARI H; p <0.001, and EPS; p <0.05) in HepG2 cells (Fig. 3F). Similarly, AKR1B1 inhibition reduced p-Akt (NARI; p <0.01& EPS; p <0.05), cMYC (NARI; p <0.05& EPS; p <0.05), and glucose transporter 1 (NARI; p <0.001& EPS; p <0.05) in PLC/PRF-5-AKR1B1+ cells (Fig. 3B).

Obstructing the polyol flux results in suppression of the Warburg effect and lipid accumulation

Our preliminary data indicated that aldose reductase inhibition prevented the overexpression of KHK and inhibited

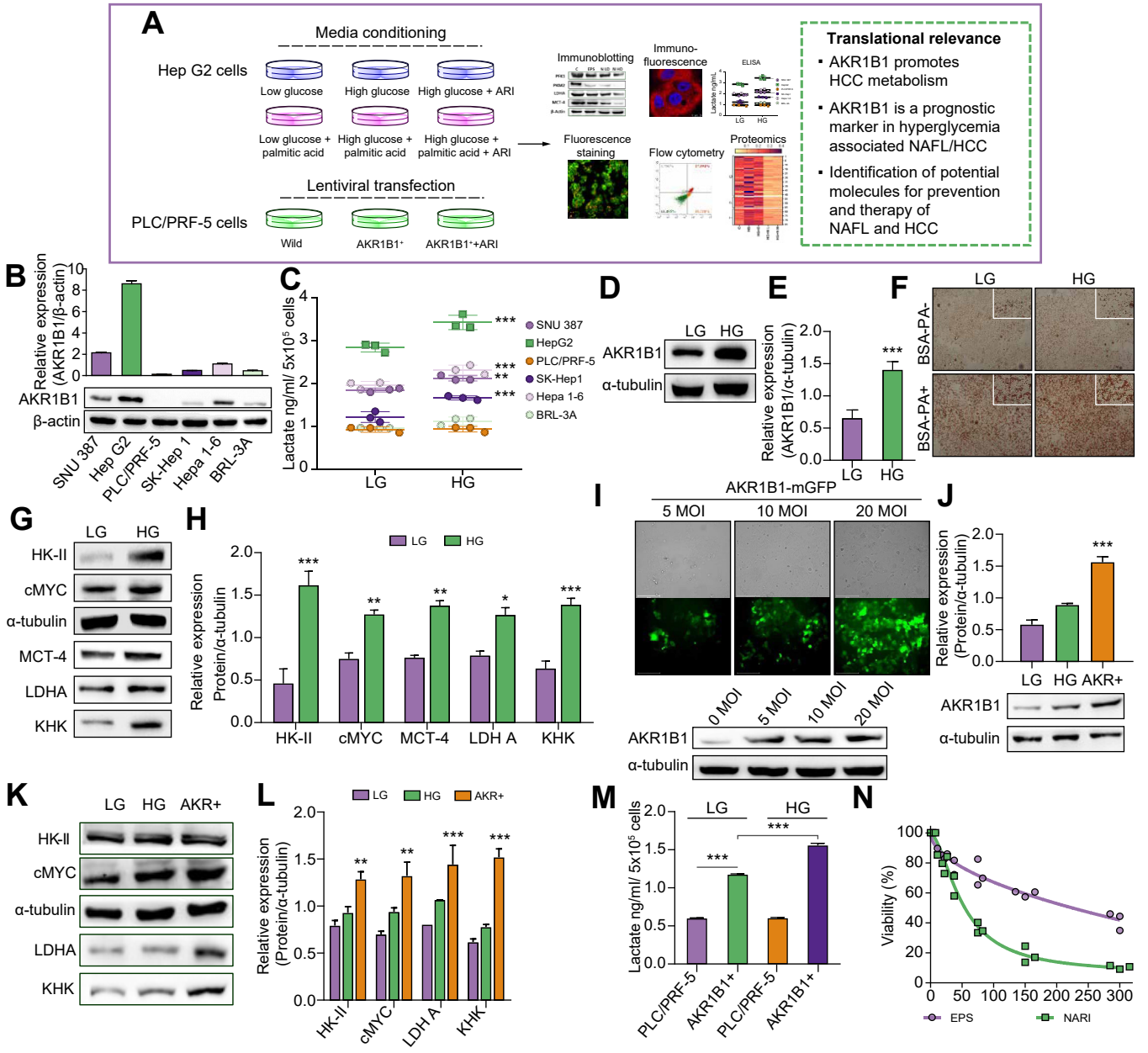

Fig. 2. Hyperglycemia or lentiviral transfection-mediated overexpression of AKR1B1 and metabolic reprogramming in human HCC cell lines. (A) Pictorial representation of study outline. (B) Immunoblotting represents the differential expression of AKR1B1 in hepatic cancer cell lines. (C) Graphical representation of lactate secretion in culture media after 24 h of maintenance in LG (2 g/L glucose) and HG (4.5 g/L glucose) (each dot represents individual data and the line inside the box represent median values. Level of significance: $^{**}p$ <0.01, $^{***}p$ <0.001; (two-way ANOVA followed by Tukey test). (D,G) Immunoblotting represents the differential expression of AKR1B1 and metabolic proteins like HK-II, cMYC, MCT-4, LDHA, and KHK in the HepG2 cell line. (E,H) Densitometric analysis of AKR1B1, HK-II, cMYC, MCT-4, LDHA, and KHK immunoblots (each bar represents mean ± SEM). Level of significance: $^{*}p$ <0.05, $^{**}p$ <0.01, $^{***}p$ <0.001; (one-way ANOVA followed by Tukey test). (F) Oil Red O staining of HepG2 cell line insulted with BSA-palmitate under LG and HG. (G) Immunofluorescence and immunoblotting assay depicting overexpression of AKR1B1 in PLC/PRF-5 cells using lentiviral particle. (J,K) Immunoblotting represents the differential expression of AKR1B1 and metabolic proteins like HK-II, cMYC, LDHA, and KHK. (J,L) Densitometric analysis of AKR1B1, HK-II, cMYC, LDHA, and KHK (each bar represents mean ± SEM). Level of significance: $^{*}p$ <0.05, $^{**}p$ <0.01, $^{***}p$ <0.001; (one-way ANOVA followed by Tukey test). (M) Graphical representation of lactate secretion in culture media of PLC/PRF-5 and AKR+ cell lines after 24 h of maintenance in LG (2 g/L glucose) and HG (4.5 g/L glucose) (each bar represents mean ± SEM). Level of significance: $^{***}p$ <0.001; (one-way ANOVA followed by Tukey test). (N) Line plot displaying percentage viability of PLC/PRF-5-AKR1B1+ cells upon treatment with EPS and NARI-29 at varying concentrations. BSA-PA, Bovine serum alcohol-palmitic acid; EPS, Epalrestat; HCC, hepatocellular carcinoma; HG, high glucose; LG, low glucose; MOI, multiliplicity of infection; NAFL, non-alcoholic fatty liver.

the rerouting of fructose to the glycolytic pathway. Furthermore, immunoblotting and metabolomics analysis revealed that AKR1B1 inhibition with EPS or NARI-29 substantially reduced the expression of HK-II (HepG2: NARI L, NARI H; p <0.001, and EPS; p <0.05 and PLC/PRF-5-AKR1B1+: NARI and EPS; p <0.01), which converts glucose to glucose-6-phosphate. As a result,

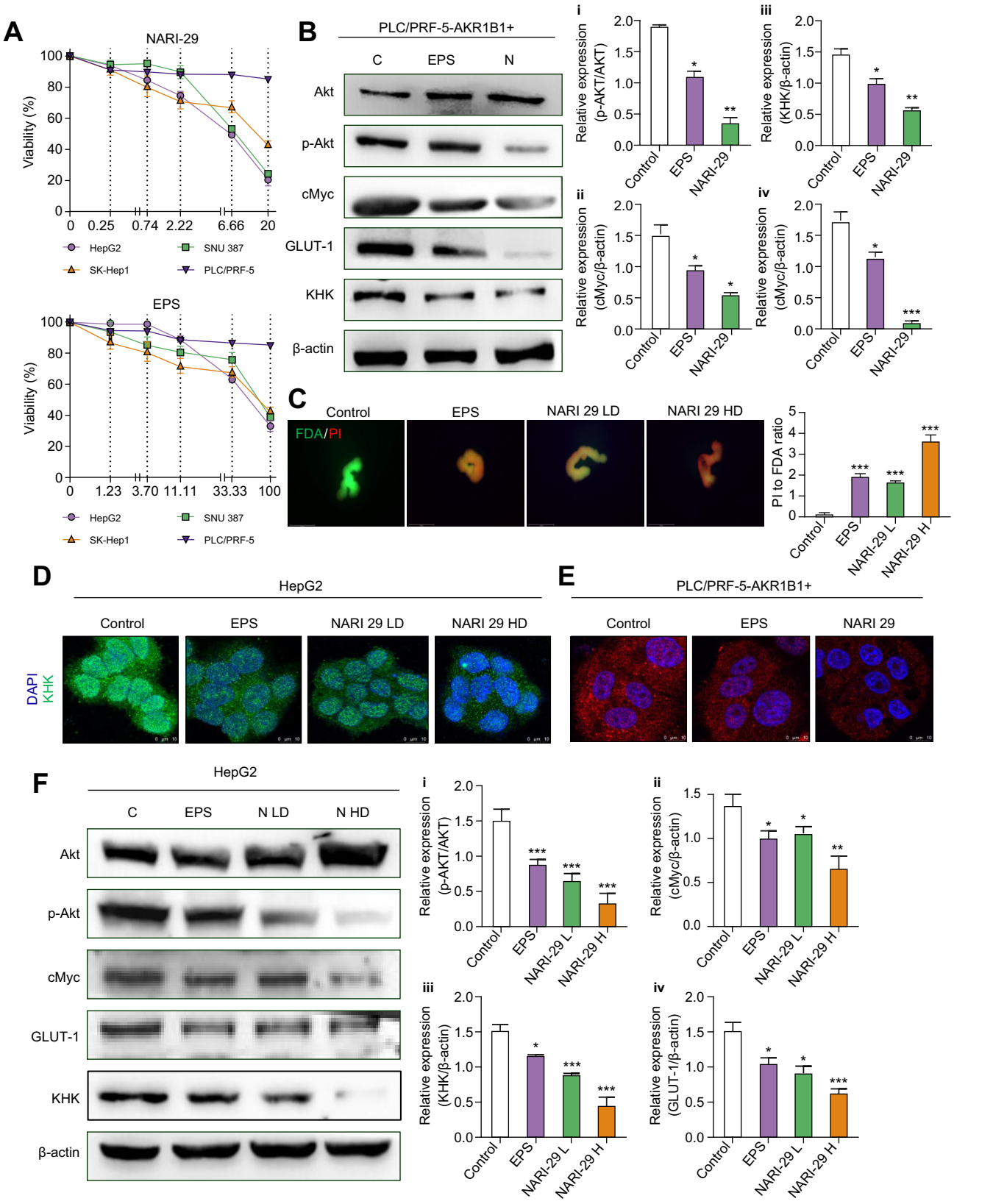

Fig. 3. AKR1B1 inhibition reverses polyol flux and GLUT-1 expression. (A) Line plot showing percentage cell viability of NARI-29 and EPS in the different hepatic cancer cell lines. Representative immunoblots and bar graphs show differential expression of AKT, pAKT, cMYC, GLUT-1, and KHK on (B) PLC/PRF-5-AKR+ cell line and (F) HepG2 cell line (HG: 4.5 g/L) (each bar represents mean ± SEM). Level of significance: $^{*}p$ <0.05, $^{**}p$ <0.01, $^{***}p$ <0.001; (one-way ANOVA followed by Tukey test). (C) Representative images of fluorescence diacetate and propidium iodide dual staining assay depicting live and dead cells in HepG2 spheroid

glucose-6-phosphate was reduced (HepG2: NARI L, NARI H; p <0.05). Consequently, there was a noticeable decrease in phosphofructokinase muscle (PFKM) (HepG2: NARI L, NARI H; p <0.001, and EPS; p <0.05 and PLC/PRF-5-AKR1B1+: NARI and EPS; p <0.01), which converts fructose 6-phosphate to fructose 1,6-bisphosphate. This led to reduced levels of fructose 1, 6-bisphosphate (n.s), and phosphoenolpyruvate (HepG2: NARI L, NARI H; p <0.05).

This initial suppression of the glycolytic phase resulted in decreased expression of pyruvate kinase M2 (PKM) (HepG2: NARI L, NARI H, and EPS; p <0.001 and PLC/PRF-5-AKR1B1+: NARI; p <0.01 and EPS; p <0.05), responsible for pyruvate production, thereby corroborating reduced pyruvate conversion. The Warburg effect is characterized by production of lactate and acidification of the microenvironment. There was a notable reduction in LDHA (HepG2: NARI H; p <0.001 and PLC/PRF-5-AKR1B1+: NARI; p <0.01 and EPS; p <0.05), resulting in decreased intracellular lactate production (HepG2: NARI L, NARI H; p <0.05) and subsequently reduced expression of MCT-4 (HepG2: NARI L; p <0.01, NARI H; p <0.001, and EPS; p <0.05 and PLC/PRF-5-AKR1B1+: NARI; p <0.01 and EPS; p <0.05). These findings collectively indicated a reversal of the Warburg effect in hepatic cancer cell lines. Furthermore, this reversal was confirmed by a decrease in extracellular acidification, as evidenced by reduced lactate concentrations in the culture media (HepG2: NARI L; p <0.05, NARI H; p <0.05, and EPS; p <0.001) (Figs 4A, C and S6). These results highlight a profound impact on the metabolic reprogramming in hepatic cancer cells following AKR1B1 inhibition.

Accumulating lipid globules and forming fatty liver is one of the early events occurring in MASLD-associated hepatocarcinogenesis. Besides inhibiting the Warburg effect, AKR1B1 inhibition-mediated impairment in glycolytic flux reduced the formation of lipid globules estimated by ORO staining. As shown in Fig. 4B, AKR1B1 inhibition with EPS and NARI-29 significantly (p <0.001) reduced the hyperglycemia-mediated formation of lipid globules in HepG2 cells. Moreover, treatment dramatically inhibited (p <0.001) BSA-palmitic acid-mediated oil deposition, indicating the role of AKR1B1 in promoting MASLD via metabolic reprogramming.

AKR1B1 inhibition modulated mitochondrial dynamics and initiated apoptosis in hepatic cancer cells

Mitochondrial dynamics (mitochondrial fusion or fission) balances the energy requirement and supply to cancer cells. Herein we investigated the expression of fusion and fission proteins after AKR1B1 inhibition. As depicted in Fig. 5C, NARI-29 treatment increased the expression of MFN-1 and decreased the expression of DRP-1 (dynamin related protein 1). The ratio of MFN-1 over DRP-1 was significantly increased in NARI-29 low-dose (p <0.05) and high-dose (p <0.001) groups, while only a slight increase in the ratio was observed with EPS treatment. The data indicates that aldose reductase inhibition leads to mitochondrial fusion in HepG2 cells. Further, to analyze the mitochondrial network in confocal images of MitoTracker staining, we have employed mitochondria Analyzer plugging in ImageJ software. As shown in Fig. 5D, E, the increased (p <0.001) mitochondrial aspect ratio in EPS and NARI-29 treatment groups indicates that mitochondrial fusion was augmented by AKR1B1 inhibition.

Further, we observed that mitochondrial fusion resulted in a significant increase in superoxide generation (p <0.001) (Fig. 5F,H) and impairment of mitochondrial membrane potential in treatment groups (Fig. 5G, I). As a result, we observed an increased ratio of Bax to BCL-2 (EPS; p <0.05, NARI L; p <0.01, and NARI H; p <0.001) in treatment groups, indicating the initiation of apoptosis (Fig. 5J). Relating to this, immunofluorescence data suggests that the localization of HK-II to mitochondria was high in HepG2 cells cultured in HG, and treatment with EPS and high-dose NARI-29 drastically reduced (p <0.01) the association of HK-II with mitochondria (Fig. 5A, B). HK-II is a mitochondrial permeability transition pore-associated protein, which negatively regulates pore opening and apoptosis in cancer cells.[21] Based on proteomics data, it appears that inhibiting AKR1B1 under hyperglycemia not only disrupts the association between HK-II and mitochondria, but also increases the expression of proteins in the mitochondrial permeability transition pore complex, including voltage-dependent anion channel 1, 2 and 3, adenine nucleotide translocase, and inorganic phosphate carrier in HepG2 cells (Fig. S7). This ultimately leads to the opening of mitochondrial pores and triggers apoptosis.

AKR1B1 inhibitors modulate the TCA cycle to deplete ATP and induce apoptosis in hepatic cancer cells

The proteomics data revealed that proteins involved in glucose metabolism, the pentose phosphate pathway, and the tricarboxylic acid (TCA) cycle were predominantly upregulated in HepG2 cells cultured in HG media compared to normal glucose media. Similar to immunoblotting data, proteomics analysis revealed that AKR1B1 inhibition with EPS (50 μM) or NARI-29 (10 and 20 μM) decreased the relative abundance of metabolic markers in the HepG2 cell line (Fig. 6B). Furthermore, our data suggests that the altered mitochondrial dynamics following NARI-29 and EPS treatment are associated with impairment of the TCA cycle in the HepG2 cell line. As shown in Fig. 6C, HG media increased the relative abundance of the TCA enzymes, pyruvate dehydrogenase (1.04-fold), citrate synthase (1.32-fold), aconitase 1 (1.74-fold), isocitrate dehydrogenase (1.78-fold), oxoglutarate dehydrogenase (1.68), succinyl-CoA ligase ADP forming subunit beta (1.25), succinate dehydrogenase (1.38-fold), fumarate hydratase (1.61-fold), malate dehydrogenase (1.82-fold), and pyruvate carboxylate (1.93-fold), indicating increased TCA cycle activity in hyperglycemia. However, treatment with EPS (50 μM) and NARI-29 (10 and 20 μM) reduced the relative abundance of all the enzymes involved in the TCA cycle, hampering ATP production. As shown in Fig. 6A, intracellular ATP decreased significantly after EPS (50 μM; p <0.01) and NARI-29 (20 μM; p <0.001) treatment, which leads to cleavage of PARP

culture upon AKR1B1 inhibition with NARI-29 (LD: 10 μM and HD: 20 μM) and EPS (50 μM) (each bar represents mean ± SEM). Level of significance: $^{***}p$ <0.001; (one-way ANOVA followed by Tukey test). Representative immunofluorescence images for KHK on (D) HepG2 cell line (HG: 4.5 g/L) and (E) PLC/PRF-5-AKR+ cell line. EPS: Epalrestat, LD: Low dose, and HD: High dose.

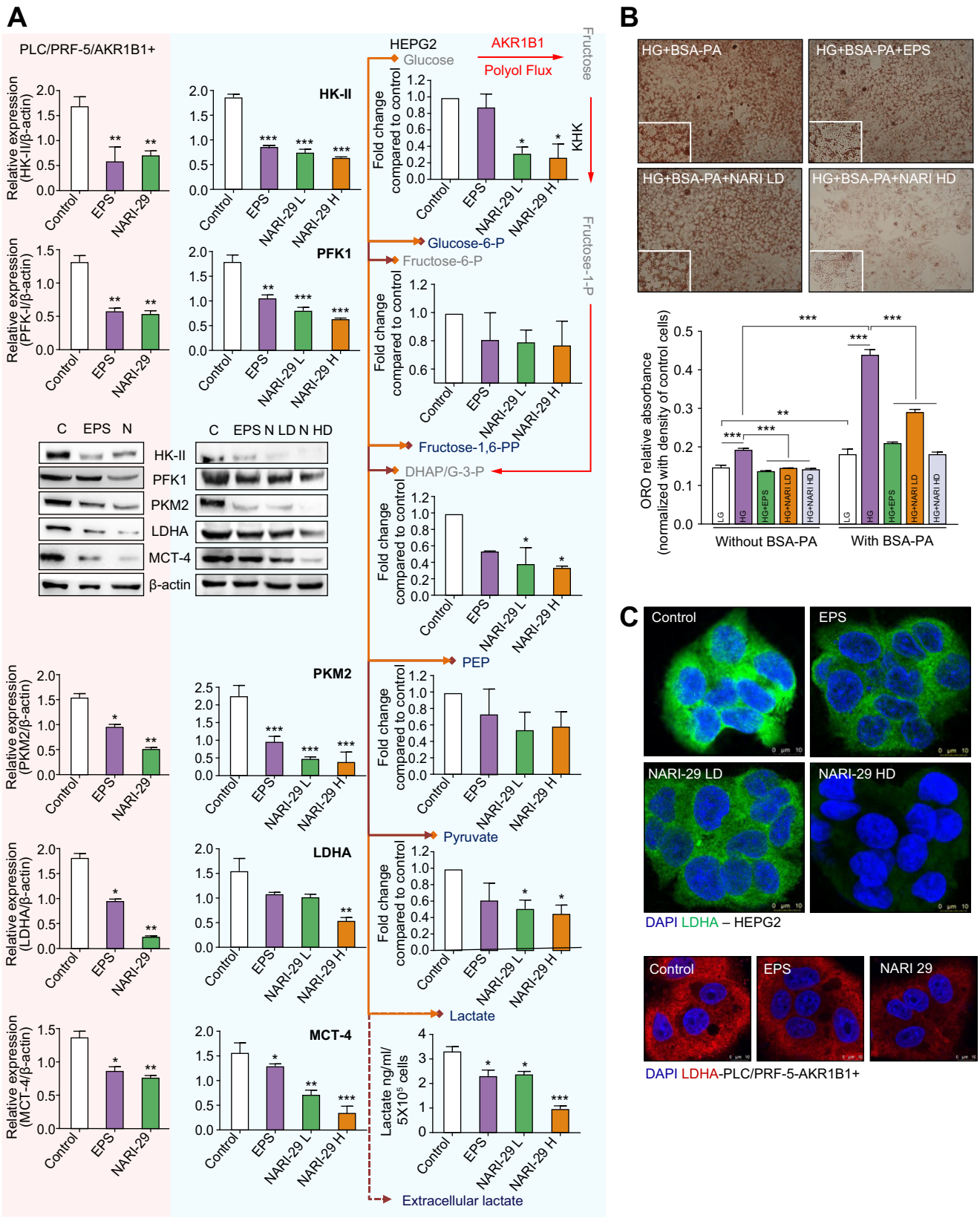

Fig. 4. Reversal of Warburg effect through AKR1B1 inhibition. (A) Representative immunoblots and bar graphs show differential expression of glycolytic markers HK-II, PFK1, PKM2, LDHA, and MCT-4 on HepG2 cell line (HG: 4.5 g/L) and PLC/PRF-5-AKR+ cell line coupled with metabolomics data for glucose-6 phosphate, fructose 1, 6 bisphosphate, phosphoenolpyruvate, lactate and extracellular lactate in HepG2 cell line upon AKR1B1 inhibition with NARI-29 (LD: 10 μM and HD: 20 μM) and EPS (50 μM) for 24 h (each bar represents mean ± SEM). Level of significance: $^{*}p$ <0.05, $^{**}p$ <0.01, $^{***}p$ <0.001; (one-way ANOVA followed by Tukey test). (B) Representative images of ORO staining about oil globule deposition (captured using 200X magnification) and bar graph showing ORO

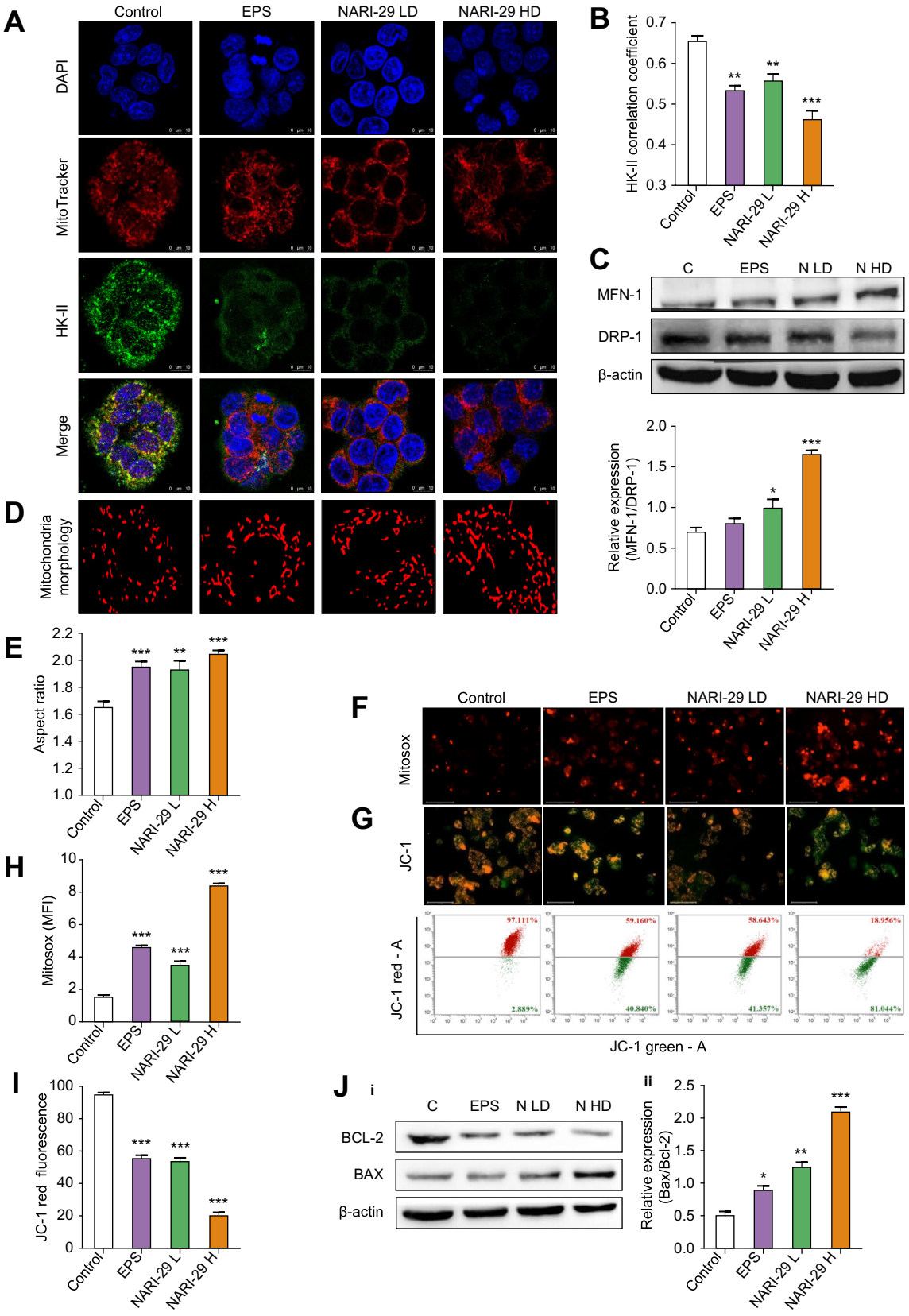

relative absorbance in HepG2 cell line after 24 h of insult with BSA-palmitate under hyperglycemia (4.5 g/L glucose) with or without AKR1B1 inhibition with NARI-29 (LD: 10 μM and HD: 20 μM) and EPS (50 μM) (each bar represents mean ± SEM). Level of significance: $^{*}p$ <0.05, $^{**}p$ <0.01, $^{***}p$ <0.001; (two-way ANOVA followed by Tukey test). (C) Representative immunofluorescence images for LDHA in HepG2 and PLC/PRF-5-AKR+ cell line (HG: 4.5 g/L). BSA-PA, Bovine serum alcohol-palmitic acid; EPS, Epalrestat; HD, high dose; HG, high glucose;LD: Low dose; ORO, Oil red O staining.

(p <0.001, Fig. 6F) and apoptosis in HepG2 cells. Further, AO/EB (Fig. 6D), FDA/PI (Fig. S8), and Annexin V/PI (Fig. 6E) staining confirmed the significant induction of apoptosis by EPS and NARI-29 treatments.

AKR1B1 inhibition reverses HFrD-aggravated DEN-induced MASLD in mice

The pharmacokinetic properties of NARI-29 in BALB/c mice were impressive at doses of 25 mg/kg and 50 mg/kg (Fig. 7B). The drug exhibited a Cmax of 14.57 and 26.7 μg/ml at the respective doses, with a half-life of 3.3 h (Fig. S9A–D). Further, we show that HFrD feeding for 15 weeks combined with diethylnitrosamine (DEN) administration induces significant (p <0.001) pathologic liver transformations, such as increased liver index (Fig. 7F), aspartate aminotransferase (Fig. 7G), alanine aminotransferase (Fig. 7H), and serum triglycerides (Fig. 7H), which were associated with increased blood glucose levels (Fig. 7E, p <0.001), indicating the role of hyperglycemia in functional and structural alterations in the liver. As shown in Fig. 7D, body weight change in the HFrD+DEN group was higher than in the control group though there was no significant difference. Histopathological evaluation using H&E and ORO staining revealed fat droplet deposition in hepatocytes in the HFrD+DEN group (Fig. 7D). However, treatment with aldose reductase inhibitors EPS and NARI-29 at a dose of 50 mg/kg/day for 21 days significantly reversed the elevated hepatic enzymes, serum triglycerides, and hepatic fat deposition with glycemic control.

AKR1B1 inhibition modulates glucose metabolism to prevent precancerous hepatocyte formation

Correlating the *in vitro* findings, hyperglycemia induced by HFrD feeding augmented the polyol flux in the liver indicated by increased expression of AKR1B1 in mouse liver (Fig. 8A, C) and plasma (Fig. 8B, p <0.001). Significant expression changes in cMyc (p <0.05), AKR1B1 (p <0.001), and KHK (p <0.01)) were observed in the HFrD+DEN group compared to the control group (Fig. 8C). Other glycolytic markers (PFKM [p <0.01], PKM [p <0.001], and LDHA [p <0.01]) and a lactate transporter (MCT-4 [p <0.01]) were also upregulated in the HFrD-DEN group (Fig. 8F). This metabolic modulation increased the expression of the oncogenic marker Ki67 (Fig. 8G) and CD44 (Fig. 8A), and downregulated the adhesion marker E-cadherin (Fig. 8E) in hepatocytes, promoting carcinogenesis. Our data indicate that the aggravation of polyol and glycolytic flux through AKR1B1 contributes significantly to precancerous hepatocyte formation. However, treatment with EPS and NARI-29 significantly reduced the HFrD+DEN-induced overexpression of AKR1B1 (tissue: EPS; p <0.05 and NARI-29; p <0.001 and plasma: EPS; p <0.05 and NARI-29; p <0.01), KHK (EPS; p <0.001 and NARI-29; p <0.01), and cMyc (EPS; p <0.05 and NARI-29; p <0.01). Further, we have shown that the AKR1B1 inhibition reduced glycolytic flux and the expression of a lactate transporter in the mouse liver (PFKM [NARI-29; p <0.05], PKM [EPS; p <0.01 and NARI-29; p <0.001], LDHA [EPS; p <0.01 and NARI-29; p <0.01], and MCT-4 [NARI-29; p <0.01]). As a result of reversing aberrant metabolism, AKR1B1 inhibition prevented precancerous transformation, evidenced by decreased expression of Ki67 and CD44 and increased expression of E-cadherin compared to the disease group.

Discussion

Metabolic switching is an adaptive mechanism for cancer development and aggravation.[22] Normal cells rely on oxidative phosphorylation for survival and energy production. However, cancer cells show a dual phenotype; in normal conditions, cancer cells tend to be in a glycolytic phenotype,[23] whereas they immediately switch their metabolism to oxidative phosphorylation in response to external stimuli that induce oxidative stress. Once the stimuli are removed, they return to their glycolytic phenotype (Warburg effect).[24,25] Similarly, an increased glycolytic metabolic phenotype was observed in MASH-associated HCC progression. This metabolic switching is prominent in patients with diabetic co-morbidity. Identifying a target responsible for this metabolic switching and disease pathology will help to screen potential therapeutic molecules. Cumulated evidence indicates a role of AKR1B1 and the polyol pathway in metabolic modulation, especially in diabetic complications.[26] However, there is no proof of the relation between AKR1B1 and the Warburg effect in MASLD-mediated HCC.

Studies show that AKR1B1 can reroute glucose to the polyol pathway to generate sorbitol, which is converted to fructose by the sorbitol dehydrogenase enzyme.[27] Recent reports revealed that increased fructose formation through polyol flux promotes the Warburg effect in cancer cells.[9] Interestingly, our data suggested a stage-specific increase in AKR1B1 in plasma and tissues of patients with MASLD/MASH, MASH-associated HCC, HCC, and DM+HCC, indicating that AKR1B1 is a disease-progressive marker in HCC which is more prominent in patients with hyperglycemia. Cell-based assays showed that AKR1B1 expression

Fig. 5. AKR1B1 inhibition promotes mitochondrial fusion. (A) Representative immunofluorescence images for HK-II and Mitotracker staining in HepG2 cell line (HG: 4.5 g/L) upon AKR1B1 inhibition with NARI-29 (LD: 10 μM and HD: 20 μM) and EPS (50 μM). (B) Graphical representation of HK-II correlation coefficient (each bar represents Mean ± SEM). Level of significance: $^{**}p$ <0.01, $^{***}p$ <0.001; (one-way ANOVA followed by Tukey test). (C) Representative immunoblots and bar graphs showing differential expression of MFN-1/DRP-1 ratio in HepG2 cell line (HG: 4.5 g/L) (each bar represents mean ± SEM). Level of significance: $^{*}p$ <0.05, $^{***}p$ <0.001; (one-way ANOVA followed by Tukey test). (D) Representative images for mitochondrial network in single cell generated from mitochondria Analyser ImageJ plugin. (E) Bar graph showing the mitochondrial aspect ratio upon AKR1B1 inhibition with NARI-29 (LD: 10 μM and HD: 20 μM) and EPS (50 μM) (each bar represents mean ± SEM). Level of significance: $^{**}p$ <0.01, $^{***}p$ <0.001; (one-way ANOVA followed by Tukey test). (F) Representative images for mitosox staining assay. (G) Representative images for JC-1 staining and a dot plot showing JC-1 aggregated (red) and monomers (green) were performed using flow cytometry. (H) Bar graph showing mean fluorescence intensity of mitosox upon AKR1B1 inhibition with NARI-29 (LD: 10 μM and HD: 20 μM) and EPS (50 μM) (each bar represents mean ± SEM). Level of significance: $^{***}p$ <0.001; (one-way ANOVA followed by Tukey test). (I) Graphical representation of JC-1 red fluorescence upon AKR1B1 inhibition with NARI-29 (LD: 10 μM and HD: 20 μM) and EPS (50 μM). (each bar represents mean ± SEM). Level of significance: $^{***}p$ <0.001; (one-way ANOVA followed by Tukey test) (I) Representative immunoblots and bar graphs showing the ratio of Bax to BCL-2 in the HepG2 cell line (each bar represents mean ± SEM). Level of significance: $^{*}p$ <0.05, $^{**}p$ <0.01, $^{***}p$ <0.001; (one-way ANOVA followed by Tukey test). EPS: Epalrestat, LD: Low dose, and HD: High dose.

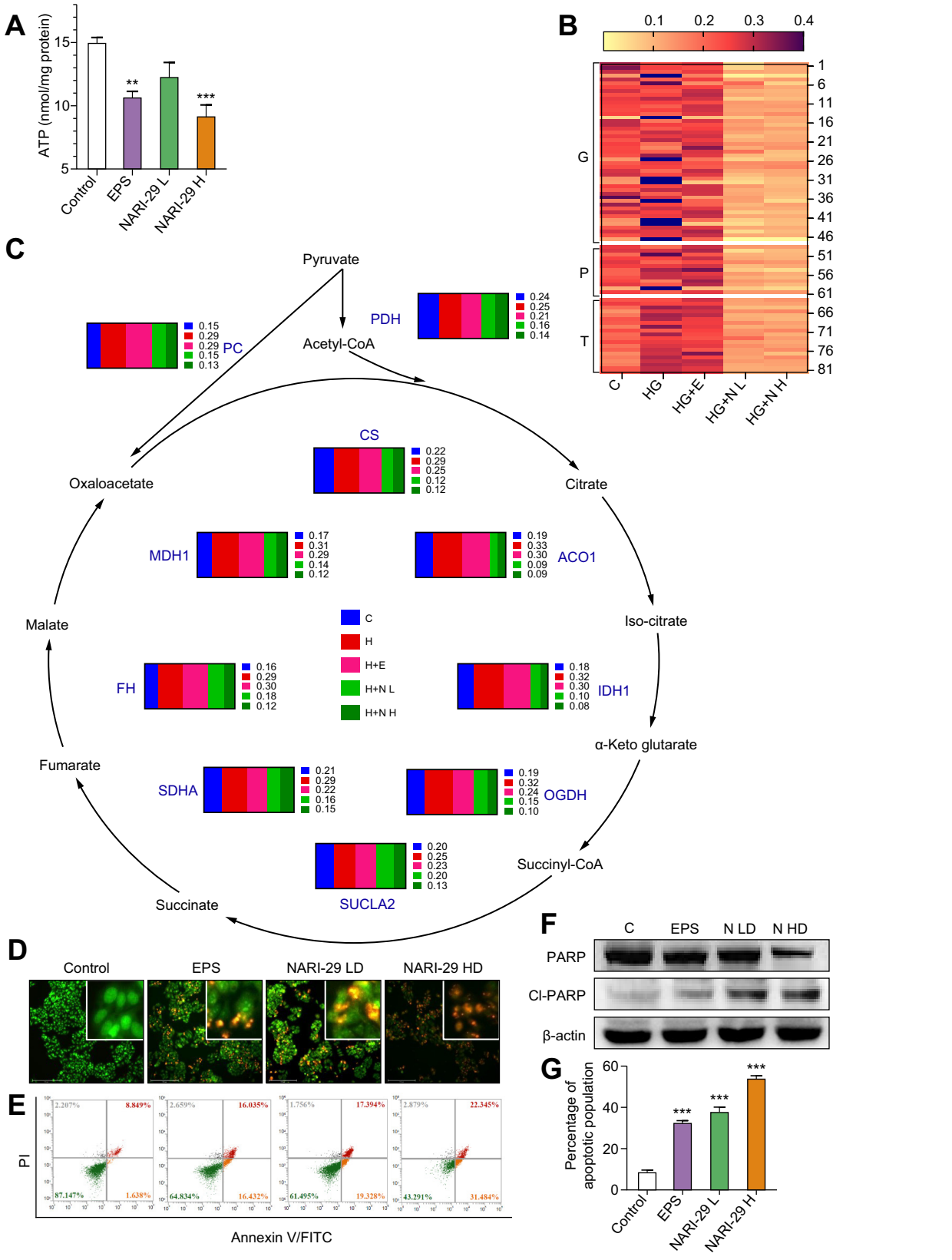

Fig. 6. AKR1B1 inhibition impairs the TCA cycle and depletes ATP to induce apoptosis. (A) Graphical representation of ATP content measured using ELISA (each bar represents mean ± SEM). Level of significance: $^{**}p$ <0.01, $^{***}p$ <0.001; (one-way ANOVA followed by Tukey test) (B) Heat map for change in metabolic proteins analyzed by proteomics in HepG2 cell line. (C) Pictorial representation for expression of TCA cycle enzymes upon AKR1B1 inhibition with NARI-29 (LD: 10 μM and HD: 20 μM) and EPS (50 μM) (C: Control, H: High glucose). (D) Representative images of acridine orange and ethidium bromide dual staining. (E) Dot plot showing annexin V/PI dual staining to confirm apoptosis performed using flow cytometry. (F) Representative immunoblots and (G) bar graph showing differential expression of PARP and CL-PARP upon AKR1B1 inhibition with NARI-29 (LD: 10 μM and HD: 20 μM) and EPS (50 μM) (each bar represents mean ± SEM). Level of significance: $^{*}p$ <0.05, $^{**}p$ <0.01, $^{***}p$ <0.001; (one-way ANOVA followed by Tukey test). LD: Low dose, HD: High dose, EPS: Epalrestat, H: High glucose, and C: Control.

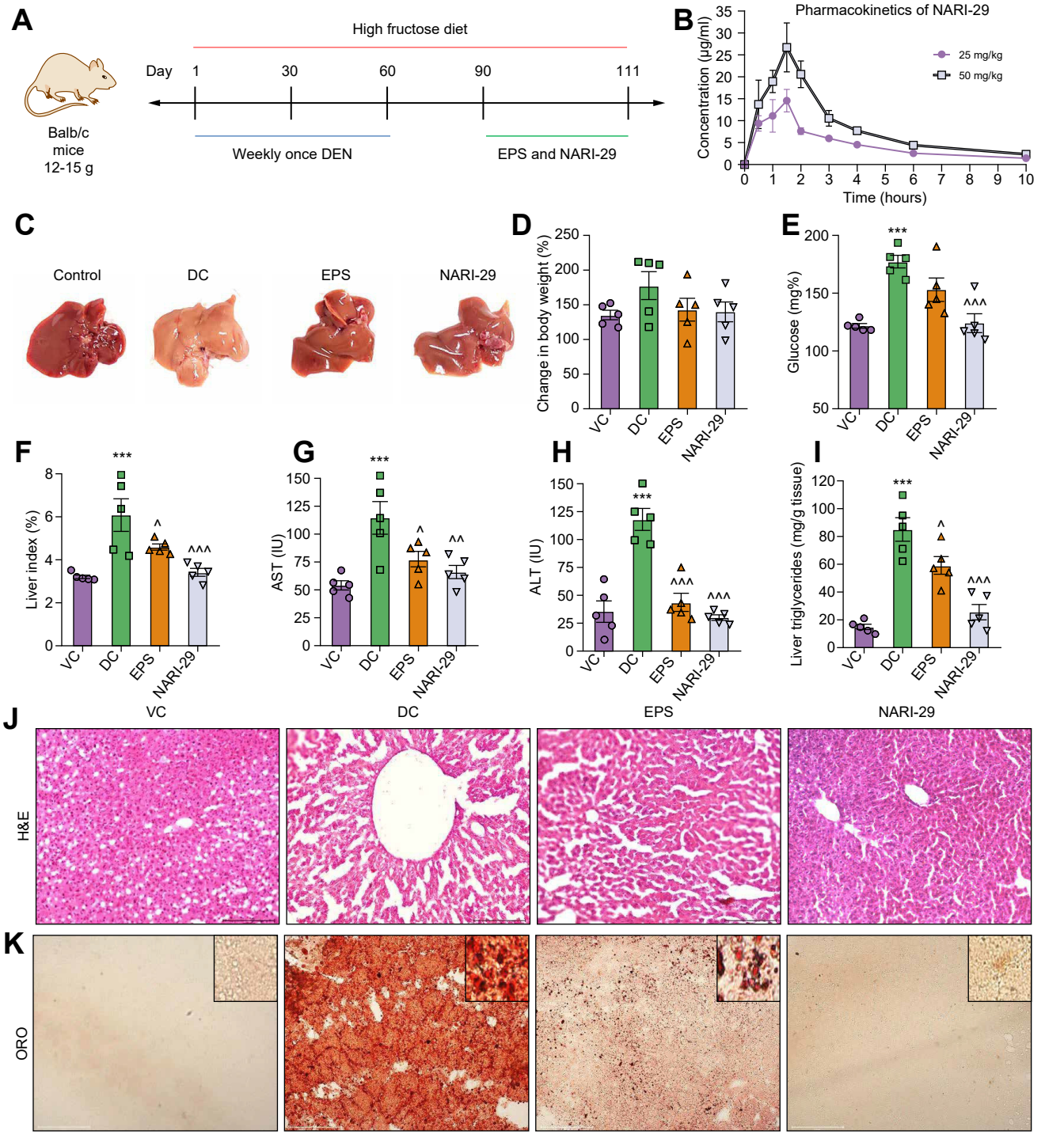

Fig. 7. Aldose reductase inhibition reverses high fructose-aggravated DEN-induced MASLD in mice. (A) Pictorial representation of *in vivo* study design. (B) Line plot depicting area under the curve (plasma conc. *vs.* time) of NARI-29 (25 and 50 mg/kg). Data are represented as mean ± SEM (n = 4). (C) Representative liver images of various experimental groups. Bar graph illustrating (D) percentage change in body weight (each bar represents mean ± SEM and each point represents individual animal data). (E) Serum glucose levels (mg%) (each bar represents mean ± SEM and each point represents individual animal data). Level of significance: $^{***}p$ <0.001 *and* $^{\sim\sim}p$ <0.001 (one-way ANOVA followed by Tukey test). (F) Liver index: liver weight/body weight (%) (each bar represents mean ± SEM and each point represents individual animal data). Level of significance: $^{***}p$ <0.001 $^{\wedge}p$ <0.05, and $^{\sim\sim}p$ <0.001) (one-way ANOVA followed by Tukey test), (G) serum AST levels (IU) (each bar represents mean ± SEM and each point represents individual animal data). Level of significance: $^{***}p$ <0.001, $^{\wedge}p$ <0.05, and $^{\sim\sim}p$ <0.01 (one-way ANOVA followed by Tukey test). (H) Serum ALT levels (IU) (each bar represents mean ± SEM and each point represents individual animal data). Level of significance: $^{***}p$ <0.001, and $^{\sim\sim}p$ <0.001; (one-way ANOVA followed by Tukey test) and (I) Liver triglyceride levels (mg/g tissue) of various experimental groups (each bar represents mean ± SEM and each point represents individual animal data). Level of significance: $^{***}p$ <0.001, $^{\wedge}p$ <0.05, and $^{\sim\sim}p$ <0.001 (one-way ANOVA followed by Tukey test). DC, disease control; DEN, diethylnitrosamine; EPS, Epalrestat; ORO, Oil red O staining; VC, vehicle control.

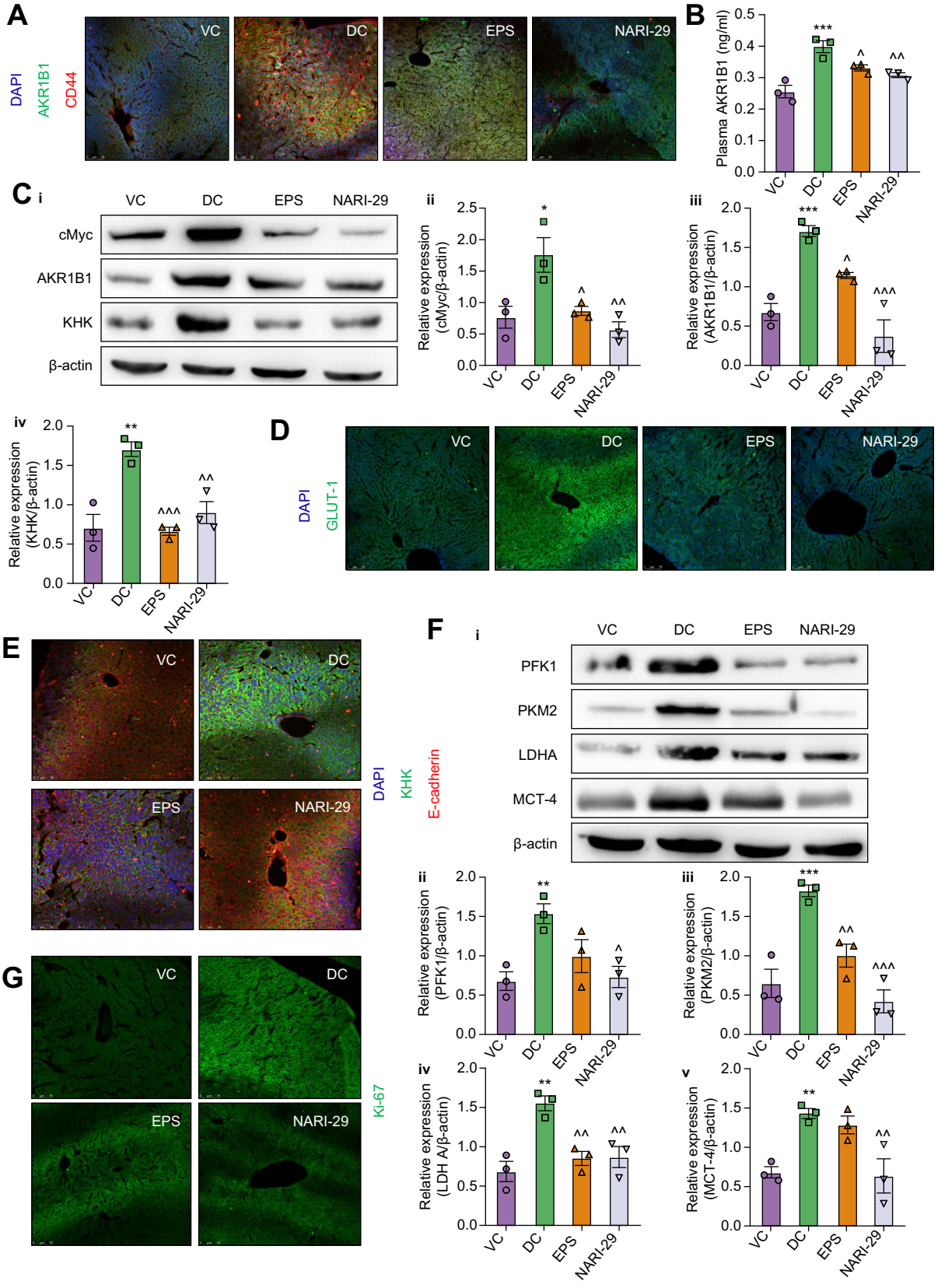

Fig. 8. Aldose reductase inhibition reverses the metabolic modulation in mouse liver. Representative immunofluorescence images for (A) AKR1B1 and CD44, (D) GLUT-1, (E) KHK and E-cadherin, and (G) Ki-67 in mouse liver tissue sections of various experimental groups. (B) Bar graph showing the expression of AKR1B1 in mouse plasma (each bar represents mean ± SEM and each point represents individual animal data). Level of significance: $^{***}p$ <0.001, $^{\wedge}p$ <0.05, and $^{\wedge\wedge}p$ <0.01 (one-way ANOVA followed by Tukey test). (C) Representative (i) immunoblots and bar graph showing differential expression of (ii) cMYC, (iii) AKR1B1, and (iv)

correlates with lactate secretion and fat deposition in HCC cell lines under hyperglycemia, indicating the role of AKR1B1 in promoting the Warburg effect and fatty liver. Further, we observed that AKR1B1 expression was upregulated in the HepG2 cell line with an increase in glucose concentration. Reports suggest that the hyperglycemia-induced overexpression of AKR1B1 drags 30% glucose from the glycolytic pathway, which is responsible for diabetic complications.[28]

Besides the enzymatic role, AKR1B1 binds to Akt, which can activate cMyc, a key regulator of metabolic pathways.[15] We have shown that HG is associated with increased expression of the glycolytic enzymes HK-II, KHK, and LDHA. As the polyol pathway consumes NAD+ and converts it to NADH,[29] lactate dehydrogenase activity moves towards lactate production, which increases the expression of MCT-4. Further, lentiviral-mediated stable overexpression of AKR1B1 in PLC/PRF-5 cells (AKR1B1 low expression) resulted in a glycolytic phenotype with increased expression of cMyc, HK-II, KHK, and LDHA, with increased lactate secretion. This data demonstrates, for the first time, the role of AKR1B1 in metabolic modulation and lactate secretion in HCC. Similar metabolic changes also occur in hepatocytes in fatty livers. The vital glycolytic enzymes (HK-II, PFKM, and PKM) were increased in the liver of high-fat diet-compared to regular chow-fed mice.[30] Another study reported that overexpression of HK-II and PKM promoted liver growth and liver steatosis related to carcinogenesis in the fatty liver.[31] Similarly, our data implicated AKR1B1 in promoting MASLD formation via metabolic reprogramming.

Further, AKR1B1 inhibition with the standard inhibitor EPS and our investigational molecule NARI-29 inhibited glycolytic flux in HepG2 and PLC/PRF-5-AKR1B1+ cells. The inhibition of the Warburg effect is evidenced by decreased lactate secretion in culture media, and the prevention of fatty liver formation is evidenced by decreased lipid globules. It has been reported that targeting the Warburg effect is an attractive strategy for treating HCC.[22] The most recent report by Wang *et al.*, 2022 stated, "*Saturation of the mitochondrial NADH shuttles drives aerobic glycolysis in proliferating cell*[32]". Hence, the metabolic shifting of cancer cells warrants a dual targeting of oxidative phosphorylation and the Warburg effect for effective cancer treatment. Primarily mitochondrial dynamics govern the metabolic state of cancer cells. Fused mitochondria were observed in cells with an oxidative phenotype, while fission was observed in the glycolytic phenotype.[33] AKR1B1 inhibition resulted in mitochondrial fusion, which increased mitochondrial superoxide generation and impaired membrane potential. Moreover, our proteomics data revealed that AKR1B1 inhibition using EPS or NARI-29 reversed the upregulation of TCA cycle enzymes and reduced ATP generation in the HepG2 cell line. Cumulatively, AKR1B1 overexpression is associated with hyperglycemia-triggered metabolic reprogramming, resulting in increased lipid accumulation, proliferation, lactate secretion, and the Warburg effect in HCC.

Further, we developed a MASLD-associated hepatocarcinogenesis model using the combined administration of HFrD and DEN. This model also mimics the westernized food habit (fructose-rich food) and oxidative stress-induced chronic liver injury and carcinogenesis. It has been reported that HFrD can induce metabolic alterations in the liver[34] and chronic consumption of HFrD induces lipogenesis, oxidative stress, and inflammation in the liver.[35] Relating to these, Lanaspa *et al.* showed that the knockdown of aldose reductase or KHK protected mice from fatty liver disease induced by HG intake.[36] However, the mechanism behind HFrD-induced liver carcinogenesis is unclear. We have demonstrated that AKR1B1 participates in HFrD+DEN-induced carcinogenesis in the mouse liver. This data validates the use of AKR1B1 as a prognostic marker for early hepatic carcinogenesis. Recent studies reported that glycolysis is upregulated in hepatocarcinogenesis induced by DEN in the mouse model.[37] Similarly, we observed an increase in glycolytic markers in the livers of HFrD+DEN-treated mice, which correlates with elevated aminotransferase and triglyceride levels in the serum. Elevated serum glucose was one of the significant contributing parameters to the hepatocarcinogenesis observed in our study. Related to our research, it has been reported that fructose consumption can induce pancreatic cell damage, insulin resistance, and hyperglycemia in experimental animals.[38] Hence, elevated AKR1B1 may be an effect of hyperglycemia caused by HFrD. Further, MASLD-associated hepatocarcinogenesis was confirmed by increased expression of cMYC, Ki67, and CD44 in hepatocytes.

There are shreds of evidence for using aldose reductase inhibitors to prevent diabetes-induced micro and macrovascular complications.[39] A relevant outcome was observed in methionine- and choline-deficient diet-fed mice, wherein aldose reductase inhibition (zopol) significantly alleviated hepatic steatosis and inflammation.[40] Moreover, it has been shown that the aldose reductase-mediated lipid accumulation is through selective derepression of PPARγ and the retinoic acid receptor.[41] Our study demonstrated that AKR1B1 inhibition using EPS and/or NARI 29 reversed the MASLD induced by the combined administration of HFrD and DEN. Moreover, we have shown that AKR1B1 inhibition using EPS and/or NARI-29 reversed the metabolic alterations in mouse livers induced by HFrD+DEN, which is supported by our *in vitro* findings. Most importantly, mechanistically we demonstrated that AKR1B1 inhibition suppresses the formation of precancerous hepatocytes in mouse livers.

Overall, our data suggest that AKR1B1 regulates glycolysis and the Warburg effect in HCC under hyperglycemia, and its overexpression was correlated with early hepatocarcinogenesis in MASLD. Since the polyol pathway is restricted to cancer, diabetes, and other inflammatory diseases, effective and safe therapy can be achieved by targeting AKR1B1, especially for treating and preventing HCC in patients with diabetes. It was also concluded that the aldose reductase inhibitors EPS and NARI-29 might be potential candidates either alone or in combination with antidiabetic therapy for the prevention and treatment of diabetes-induced MASLD or HCC.

KHK in live tissue lysate (each bar represents mean ± SEM and each point represents individual animal data). Level of significance: $^{*}p$ <0.05, $^{**}p$ <0.01, $^{***}p$ <0.001, $^{\frown}p$ <0.05, $^{\frown\frown}p$ <0.01, and $^{\frown\frown\frown}p$ <0.001 (one-way ANOVA followed by Tukey test). (F) Representative (i) immunoblots and bar graph showing differential expression of (ii) PFK1, (iii) PKM2, (iv) LDHA, and (v) MCT-4 in live tissue lysate (each bar represents mean ± SEM and each point represents individual animal data). Level of significance: $^{**}p$ <0.01, $^{***}p$ <0.001, $^{\frown\frown}p$ <0.01, and $^{\frown\frown\frown}p$ <0.001 (one-way ANOVA followed by Tukey test). DC, disease control; EPS, Epalrestat; VC, vehicle control.

Abbreviations

DEN, diethylnitrosamine; DM, diabetes mellitus; EPS, epalrestat; HCC, hepatocellular carcinoma; HFrD, high-fructose diet; HG, high glucose; HK-II, hexokinase 2; KHK, ketohexokinase; LDHA, lactate dehydrogenase A; LG, low glucose; MASLD, metabolic dysfunction-associated steatotic liver disease; MASH, metabolic dysfunction-associated steatohepatitis; MCT4, monocarboxylate transporter 4; PFKM, phosphofructokinase muscle; PKM, pyruvate kinase M1/2; TCA, tricarboxylic acid.

Financial support

The authors did not receive any financial support to produce this manuscript.

Conflict of interest

The authors of this study declare that they do not have any conflict of interest.

Please refer to the accompanying ICMJE disclosure forms for further details.

Authors' contributions

VGMN: conceptualization, investigation, supervision, review & editing. DMT: methodology, visualization, review & editing SNP: conceptualization, methodology, visualization, validation, formal analysis, and writing the original draft. SJ, BR, SRP, GJK, SBJ, RMB: methodology, visualization, formal analysis, and review of the draft. KMS, PAS, VSC, RMB, and JRV: conceptualization and investigation. All authors approved the final version of the manuscript.

Data availability statement

The data associated with the results and conclusions of this publication are included in this manuscript and its supplementary files.

Ethics approval

All the experiments with human samples were performed as per the regulations of the Institutional Review Board (IRB) with approval from the Institutional Ethics Committee ILBS, Delhi (IEC/2023/98/MA05). All animal experiments were conducted according to the Committee for the Purpose of Control and Supervision of Experiments on Animals (CPCSEA) guidelines and approved by the Institutional Animal Ethical Committee (IAEC) under protocol number: NIPER/PC/2022/45.

Acknowledgments

The authors would like to acknowledge Dr. USN Murty, Director, National Institute of Pharmaceutical Education and Research Guwahati, for his support throughout the research. The authors are also thankful to the Department of Pharmaceuticals, Ministry of Chemicals and Fertilizers, Govt. of India, and National Centre for Pharmaco-engineering (NCPE) supported by DST under the DPRP scheme for providing funds to carry out the current research work.

Supplementary data

Supplementary data to this article can be found online at https://doi.org/10.1016/j.jhepr.2023.100974.

References

[1] Yuan S, Chen J, Li X, et al. Lifestyle and metabolic factors for nonalcoholic fatty liver disease: mendelian randomization study. Eur J Epidemiol 2022;37:723–733. https://doi.org/10.1007/S10654-022-00868-3/TABLES/4.

[2] Ye J, Zhuang X, Li X, et al. Novel metabolic classification for extrahepatic complication of metabolic associated fatty liver disease: a data-driven cluster analysis with international validation. Metabolism 2022;136. https://doi.org/10.1016/j.metabol.2022.155294.

[3] Liu Z, Lin C, Suo C, et al. Metabolic dysfunction–associated fatty liver disease and the risk of 24 specific cancers. Metabolism 2022;127. https://doi.org/10.1016/j.metabol.2021.154955.

[4] Rinella ME, Lazarus JV, Ratziu V, et al. A multi-society Delphi consensus statement on new fatty liver disease nomenclature. J Hepatol 2023. https://doi.org/10.1016/J.JHEP.2023.06.003.

[5] El-Serag EB, Hampel H, Javadi F. The association between diabetes and hepatocellular carcinoma: a systematic review of epidemiologic evidence. Clin Gastroenterol Hepatol 2006;4:369–380.

[6] Gallo M, Muscogiuri G, Felicetti F, et al. Adverse glycaemic effects of cancer therapy: indications for a rational approach to cancer patients with diabetes. Metabolism 2018;78:141–154. https://doi.org/10.1016/J.METABOL.2017.09.013.

[7] Habib SL, Rojna M. Diabetes and risk of cancer. ISRN Oncol 2013;2013:1–16. https://doi.org/10.1155/2013/583786.

[8] Parks SK, Mueller-Klieser W, Pouysségur J. Lactate and acidity in the cancer microenvironment. Annu Rev Cancer Biol 2020;4:141–158. https://doi.org/10.1146/annurev-cancerbio-030419-033556.

[9] Nakagawa T, Lanaspa MA, Millan IS, et al. Fructose contributes to the Warburg effect for cancer growth. Cancer Metab 2020;8. https://doi.org/10.1186/s40170-020-00222-9.

[10] Wilde L, Roche M, Domingo-Vidal M, et al. Metabolic coupling and the Reverse Warburg Effect in cancer: implications for novel biomarker and anticancer agent development. Semin Oncol 2017;44:198–203. https://doi.org/10.1053/J.SEMINONCOL.2017.10.004.

[11] Oral A, Sahin T, Turker F, et al. Relationship between serum uric acid levels and nonalcoholic fatty liver disease in non-obese patients. Medicina (B Aires) 2019;55. https://doi.org/10.3390/MEDICINA55090600.

[12] Pettinelli P, Arendt BM, Teterina A, et al. Altered hepatic genes related to retinol metabolism and plasma retinol in patients with non-alcoholic fatty liver disease. PLoS One 2018;13:e0205747. https://doi.org/10.1371/JOURNAL.PONE.0205747.

[13] Baffy G, Brunt EM, Caldwell SH. Hepatocellular carcinoma in non-alcoholic fatty liver disease: an emerging menace. J Hepatol 2012;56:1384–1391. https://doi.org/10.1016/j.jhep.2011.10.027.

[14] Tang WH, Martin KA, Hwa J. Aldose reductase, oxidative stress, and diabetic mellitus. Front Pharmacol 2012;3:87. https://doi.org/10.3389/fphar.2012.00087.

[15] Zhao J-X, Yuan Y-W, Cai C-F, et al. Aldose reductase interacts with AKT1 to augment hepatic AKT/mTOR signaling and promote hepatocarcinogenesis. Oncotarget 2017;8:66987–67000. https://doi.org/10.18632/oncotarget.17791.

[16] Syamprasad NP, Rajdev B, Jain S, et al. Molecular dissection of anti-colon cancer activity of NARI-29: special focus on H2O2 modulated NF-κB and death receptor signaling, 2023. https://doi.org/10.1080/10715762.2023.2243029; 2023.

[17] Syamprasad NP, Jain S, Rajdev B, et al. AKR1B1 inhibition using NARI-29-an Epalrestat analogue-alleviates Doxorubicin-induced cardiotoxicity via modulating Calcium/CaMKII/MuRF-1 axis. Chem Biol Interact 2023;381:110566. https://doi.org/10.1016/J.CBI.2023.110566.

[18] Syamprasad NP, Rajdev B, Jain S, et al. Pivotal role of AKR1B1 in pathogenesis of colitis associated colorectal carcinogenesis. Int Immunopharmacol 2023;119:110145. https://doi.org/10.1016/J.INTIMP.2023.110145.

[19] Reddy TN, Ravinder M, Bagul P, et al. Synthesis and biological evaluation of new epalrestat analogues as aldose reductase inhibitors (ARIs). Eur J Med Chem 2014. https://doi.org/10.1016/j.ejmech.2013.10.043.

[20] Bartha Á, Győrffy B. TNMplot.com: a web tool for the comparison of gene expression in normal, tumor and metastatic tissues. 2021, Vol 22, Page 2622 Int J Mol Sci 2021;22:2622. https://doi.org/10.3390/IJMS22052622.

[21] Roberts DJ, Miyamoto S. Hexokinase II integrates energy metabolism and cellular protection: akting on mitochondria and TORCing to autophagy. 22:2 2014 Cel Death Differ 2015;22:248–257. https://doi.org/10.1038/cdd.2014.173.

[22] Liberti MV, Locasale JW. The Warburg effect: how does it benefit cancer cells? Trends Biochem Sci 2016;41:211–218. https://doi.org/10.1016/j.tibs.2015.12.001.

[23] Zheng J. Energy metabolism of cancer: glycolysis versus oxidative phosphorylation (review). Oncol Lett 2012;4:1151–1157. https://doi.org/10.3892/ol.2012.928.

[24] Wegiel B, Vuerich M, Daneshmandi S, et al. Metabolic switch in the tumor microenvironment determines immune responses to anti-cancer therapy. Front Oncol 2018;8. https://doi.org/10.3389/fonc.2018.00284.

[25] MacFarlane M, Robinson GL, Cain K. Glucose - a sweet way to die: metabolic switching modulates tumor cell death. Cell Cycle 2012;11:3919–3925. https://doi.org/10.4161/cc.21804.

[26] Jain S, Durugkar S, Saha P, et al. Effects of intranasal azithromycin on features of cigarette smoke-induced lung inflammation. Eur J Pharmacol 2022;915. https://doi.org/10.1016/J.EJPHAR.2021.174467.

[27] Dagher Z, Park YS, Asnaghi V, et al. Studies of rat and human retinas predict a role for the polyol pathway in human diabetic retinopathy. Diabetes 2004;53:2404–2411. https://doi.org/10.2337/diabetes.53.9.2404.
[28] Banerjee S. Aldo keto reductases AKR1B1 and AKR1B10 in cancer: molecular mechanisms and signaling networks. Adv Exp Med Biol 2021;1347:65–82. https://doi.org/10.1007/5584_2021_634.
[29] Pastel E, Pointud JC, Volat F, et al. Aldo-keto reductases 1B in endocrinology and metabolism. Front Pharmacol 2012;3. https://doi.org/10.3389/FPHAR.2012.00148/FULL. AUG.
[30] Lu C, Xing H, Yang L, et al. Resveratrol ameliorates high-fat-diet-induced abnormalities in hepatic glucose metabolism in mice via the AMP-activated protein kinase pathway. Evid Based Complement Altern Med 2021;2021. https://doi.org/10.1155/2021/6616906.
[31] Feng J, Li J, Wu L, et al. Emerging roles and the regulation of aerobic glycolysis in hepatocellular carcinoma. 39:1 2020 J Exp Clin Cancer Res 2020;39:1–19. https://doi.org/10.1186/S13046-020-01629-4.
[32] Wang Y, Stancliffe E, Fowle-Grider R, et al. Saturation of the mitochondrial NADH shuttles drives aerobic glycolysis in proliferating cells. Mol Cel 2022;82:3270–3283.e9. https://doi.org/10.1016/j.molcel.2022.07.007.
[33] Ma Y, Wang L, Jia R. The role of mitochondrial dynamics in human cancers. Am J Cancer Res 2020;10:1278.
[34] Roeb E, Weiskirchen R. Fructose and non-alcoholic steatohepatitis. Front Pharmacol 2021;12:47. https://doi.org/10.3389/FPHAR.2021.634344/BIBTEX.
[35] Velázquez AM, Bentanachs R, Sala-Vila A, et al. ChREBP-driven DNL and PNPLA3 expression induced by liquid fructose are essential in the production of fatty liver and hypertriglyceridemia in a high-fat diet-fed rat model. Mol Nutr Food Res 2022;66. https://doi.org/10.1002/MNFR.202101115.
[36] Lanaspa MA, Ishimoto T, Li N, et al. Endogenous fructose production and metabolism in the liver contributes to the development of metabolic syndrome. Nat Commun 2013;4:2434. https://doi.org/10.1038/NCOMMS3434.
[37] Chen M, Lu S, Zheng H, et al. Identification of the potential metabolic pathways involved in the hepatic tumorigenesis of rat diethylnitrosamine-induced hepatocellular carcinoma via 1 H NMR-based metabolomic analysis. Biomed Res Int 2019;2019. https://doi.org/10.1155/2019/9367082.
[38] Farag MM, Ashour EH, El-Hadidy WF. Amelioration of high fructose diet-induced insulin resistance, hyperuricemia, and liver oxidative stress by combined use of selective agonists of PPAR-α and PPAR-γ in rats. Dubai Med J 2020;3:76–86. https://doi.org/10.1159/000506899.
[39] Ramana KV. Aldose reductase: new insights for an old enzyme. Biomol Concepts 2011;2:103–114. https://doi.org/10.1515/BMC.2011.002.
[40] Chen T, Shi D, Chen J, et al. Inhibition of aldose reductase ameliorates diet. induced nonalcoholic steatohepatitis in mice via modulating the phosphorylation of hepatic peroxisome proliferator-activated receptor α. Mol Med Rep 2015;11:303–308. https://doi.org/10.3892/MMR.2014.2713/HTML.
[41] Thiagarajan D, Ananthakrishnan R, Zhang J, et al. Aldose reductase acts as a selective derepressor of PPARγ and retinoic acid receptor. Cell Rep 2016;15:181. https://doi.org/10.1016/J.CELREP.2016.02.086.